Jurnal Teknologi

Full Paper

EVALUATION OF IODINE AND CALCIUM CT NUMBER IN DUAL-ENERGY COMPUTED TOMOGRAPHY (DECT) USING A FABRICATED IN-HOUSE PHANTOM

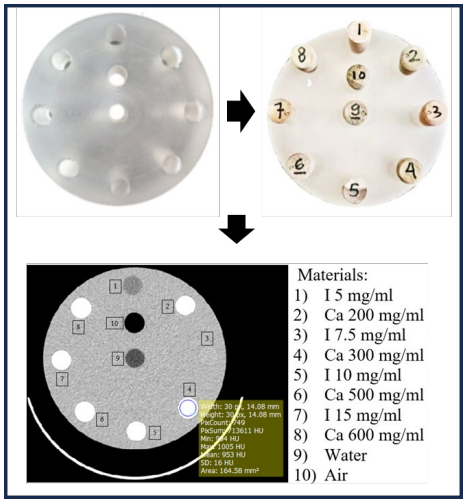
Pingki S. Dewi[a], Choirul Anam[a]*, Heri Sutanto[a], Ariij Naufal[a], Ilham Alkian[b], Adiwasono M. B. Setiawan[c], Geoff Dougherty[d]

[a]Departement of Physics, Faculty of Sciences and Mathematics, Diponegoro University, Tembalang, Semarang, Indonesia
[b]Smart Material Research Center (SMARC), Diponegoro University, Tembalang, Semarang, Indonesia
[c]Imaging Radiodiagnostics and Interventional Radiology, Santo Borromeus Hospital, Bandung, Indonesia
[d]Department of Applied Physics and Medical Imaging, California State University Channel Islands, Camarillo, CA 93012, USA

Article history
Received
30th June 2025
Received in revised form
11th October 2025
Accepted
28th October 2025
Published
1st November 2026

*Corresponding author
anam@fisika.fsm.undip.ac.id

Graphical abstract



Abstract

The aim of this study was to evaluation of iodine and calcium CT number in DECT using a fabricated In-house phantom. The phantom was made from polyester resin (PESR) mixed with methyl ethyl ketone peroxide (MEKP) as catalyst in a ratio of 300:1, with a 16 cm diameter and 5 cm height. The phantom had 10 holes, each with a diameter of 1.5 cm. Each hole was filled with water, air, iodine (with various concentrations of 5, 7.5, 10, and 15 mg/ml), and calcium (with various concentrations of 200, 300, 500, and 600 mg/ml). The phantom was scanned by an Ultrafast kV Switching DECT with a tube voltage of 80/140 kV, slice thickness of 5 mm, rotation time of 0.5 s, and tube current variations (200, 250, 300, 335, and 370 mA). Images were reconstructed to a VMI at 50, 70, and 100 keV. The CT number accuracy of VMI images was measured using IndoQCT software. Absolute percentage error (APE) was calculated from measured CT numbers and standard phantom. We found that the changes in CT numbers of iodine and calcium showed the same trend. The CT numbers for both iodine and calcium slightly increased with higher tube currents. The CT number decreased by 1.5-3 times from an energy of 50 to 100 keV. For all concentrations, the APE of CT numbers of the in-house phantom were <32% and <25% compared to the standard for iodine and calcium, respectively.

Keywords: CT number, dual energy CT, phantom, quality control, IndoQCT

© 2026 Penerbit UTM Press. All rights reserved

1.0 INTRODUCTION

Computed tomography (CT) is widely used in health services worldwide. CT images are reconstructed from a series of X-ray projections at various angles. The CT image indicates a mapping of X-ray attenuation coefficient normalized by the attenuation coefficient of water, and it is known as

DOI: https://doi.org/10.11113/jurnalteknologi.v89.25139

CT number in Hounsfield units (HU) [1-3]. X-ray attenuation coefficient depends on X-ray energy, tissue density, and tissue atomic number (Z) [4, 5]. In single energy CT (SECT), two tissues (e.g. calcium and iodine) might have similar CT numbers even though they both have different atomic numbers (e.g. calcium with Z = 20 and iodine with Z = 53) [1, 3]. To be able to differentiate two materials having different atomic numbers, a dual energy CT (DECT) has been developed. DECT uses two different X-ray spectra for image acquisition [6-8]. The technology of DECT is evolving continuously. Currently, most DECT scanners can produce a virtual monochromatic image (VMI) simulating the CT number obtained from a mono-energy CT [8-10].

The advantages of DECT in clinical use are now an active area of research. Thieme et al. [11] reported that DECT with pulmonary parenchymal iodine mapping accurately identified pulmonary perfusion, showing a close correlation with perfusion single-photon emission CT (SPECT). They concluded that this technique has the potential to enhance diagnostic accuracy. Hu et al. [12] used unenhanced dual-energy head CT (DECT) in the emergency department, analyzing the virtual non-calcium and calcium overlay images to effectively differentiate between calcification and hemorrhage. Their report demonstrated that the accuracy of DECT for hemorrhage detection was 99%, significantly surpassing the 87% accuracy of conventional CT [12]. success of such investigations depends on how accurately DECT quantifies the concentration of materials such as iodine and calcium.

DECT is a complex medical imaging system. Hence, it requires a quality control (QC) program to ensure that the image obtained is within the tolerance limit (standard). One of the parameters tested in QC for DECT is CT number accuracy [13, 14]. Generally, the CT number accuracy test in DECT is performed using a standard phantom (Gammex) having 13 rods filled with various materials representing body tissues (i.e., iodine, blood, calcium, and adipose) [11, 12]. However, the availability of standard Gammex phantom is still limited, especially in developed countries such as Indonesia. Therefore, there is a need to develop phantoms from simple and economical materials for testing accuracy of CT number in DECT.

The principle of developing phantoms is to select materials that are equivalent to human body tissues in response to X-rays [15-17]. Asiah et al [18] has successfully developed a phantom for SECT made from polyester resin (PESR). The results showed that mixing polyester resin and catalyst in a ratio of 300:1 resulted in an error of <6% compared to the standard polymethyl methacrylate (PMMA) phantom. The phantom developed by Asiah et al [18], however, can only be used for QC on SECT as it does not contain materials with different densities and atomic numbers (Z). Therefore, this study aimed to evaluation CT numbers of iodine and calcium in DECT using a fabricated In-house phantom.

2.0 METHODOLOGY

2.1 Fabrication of in-house phantom

The in-house phantom was made of PESR mixed with methyl ethyl ketone peroxide (MEKP) as a catalyst in a ratio of 300:1. Both materials were poured into the mold and stirred using a spatula for 3 minutes. The mixing time was kept short to avoid the mixture temperature soaring high which could cause cracks in the phantom. The mixture was left to dry for 2-3 days at room temperature until it became solid. After the material solidified, a turning process was carried out to obtain a phantom size of 16 cm in diameter and 5 cm in height. After that, 10 holes with a diameter of 1.5 cm were drilled for placing the iodine and calcium solutions.

2.2 Dilution of iodine and calcium solutions

Iopamidol with a concentration of 370 mg/ml was diluted to obtain iodine solutions with concentrations of 5, 7.5, 10, and 15 mg/ml. The dilution process was carried out using a magnetic stirrer for 30 minutes according to the following equation (1):

$$M_1 V_1 = M_2 (V_1 + V_2) \quad (1)$$

where M_1 is the concentration before dilution (mg/ml), M_2 is the concentration after dilution (mg/ml), V_1 is the volume of iopamidol (ml) and V_2 is the volume of aquabidest (ml).

Calcium carbonate (CaCO3) was diluted using double-distilled water to make calcium solutions with concentrations of 200, 300, 500, and 600 mg/ml. The dilution process was carried out using T25 digital ultra turrax for 30 minutes and continued with an ultrasonic cell disruptor UCD-950 (Biobase Biodustry) for 30 minutes in order to obtain a homogeneous calcium solution. The concentration of calcium was calculated using equation (2):

$$M = \frac{1000\,m}{V\,M_r} \quad (2)$$

where M is the concentration (mg/ml), m is the mass of solute (g), M_r is the relative molecular mass (g/mol) and V is the volume of solution (ml). Iodine and calcium solutions were then inserted into the phantom holes as shown in Figure 1.

DOI: https://doi.org/10.11113/jurnalteknologi.v89.25139

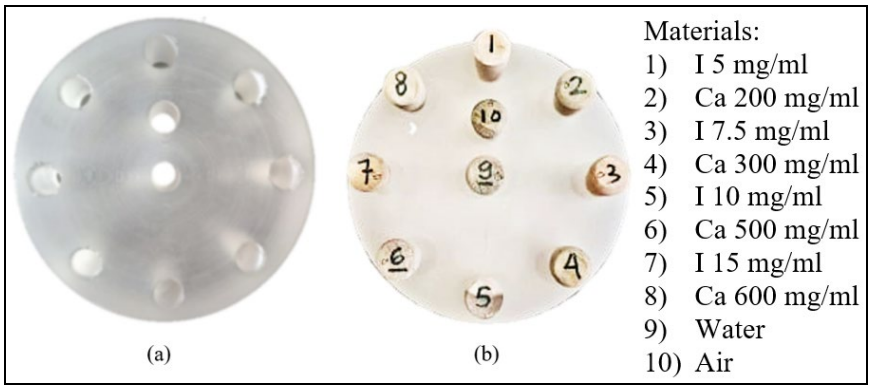


Figure 1. In-house CT phantom. (a) Before the phantom is filled with iodine and calcium solutions, and (b) After the phantom is filled with them.

2.3 Scanning the in-house phantom

In house phantoms can be used if there are no artifacts. It is ensured that the material is homogeneous and there are no air bubbles that could affect the CT number. The in-house phantom was scanned by a GE Revolution Ultrafast kV Switching DECT. The phantom position was adjusted and then imaging was performed with the scanning parameters shown in Table 1. The scanning parameters used in this study are tailored for head scanning.

Table 1. Scanning parameters

Parameters	Value
Tube voltage	80/140 kV
Tube current	200, 250, 300, 335, and 370 mA
Rotation time	0.5 s
Slice thickness	5 mm
Field of view (FOV)	25 cm
Scan type	Helical

2.4 Image analysis

After scanning is completed, the images were reconstructed to a virtual monochromatic image (VMI) at energy levels of 50, 70 and 100 keV. The VMIs were stored in the digital imaging and communications in medicine (DICOM) format and input into IndoQCT software. IndoQCT software is used to evaluate of CT images, manufactured by Diponegoro University (www.indosect.com/indoqct). In the VMIs, a region of interest (ROI) for each material to obtain the CT number as shown in Figure 2.

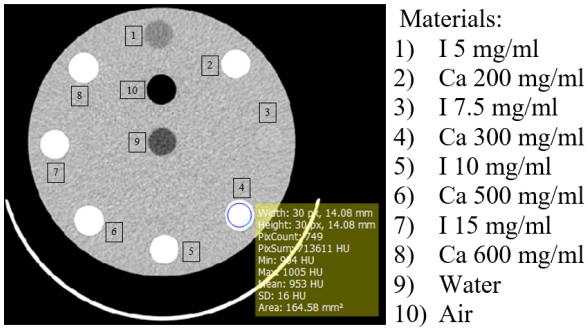


Figure 2. Region of interests (ROIs) on image of the in-house phantom

2.5 Statistical analysis

The absolute percentage error (APE) was calculated to compare the CT number between the in-house phantom and the standard phantom according to equation (3):

$$\text{APE}\ (\%) = \left|\frac{M_V - T_V}{T_V} \times 100\%\right| \quad (3)$$

where M_V is the measured value and T_V is the theoretical value shown in Table 2. The standard phantom (Gammex) has two parts, i.e., the head (20 cm diameter) and the body (40 cm diameter).

Table 2. Material specifications on a standard phantom [12, 17]

Material	CT number (HU)		
	50 keV	70 keV	100 keV
Iodine 5 mg/ml	274	127	52
Iodine 7.5 mg/ml	440	213	78
Iodine 10 mg/ml	546	256	107
Iodine 15 mg/ml	821	387	164
Calcium 200 mg/ml	1248	726	439
Calcium 300 mg/ml	1499	901	625
Calcium 500 mg/ml	1540	1057	701
Calcium 600 mg/ml	1735	1202	765

DOI: https://doi.org/10.11113/jurnalteknologi.v89.25139

3.0 RESULTS AND DISCUSSION

3.1 Images of in-house phantom

The VMI images of the phantom, scanned at energy level of 50 keV and tube voltage of 80/140 kV with various tube currents, are shown in Figure 3. It can be seen that as the tube current was increased, the noise in the image decreased. It is also seen that contrast between each material and background is constant for tube current variation. The VMI images of the phantom at tube current 300 mA and tube voltage 80/140 kV with three energy levels, are shown in Figure 4. As the energy was increased, the image noise also decreased. In addition, the contrast of the insert material changed as the VMI energy increased.

3.2 CT number of iodine

The CT number of iodine for various tube currents and energy levels are shown in Table 3. If the tube current increased, then the CT number slightly increased. And, if VMI energy level increased, then the CT number decreased. CT number also depends on the material concentration, with high concentration producing a larger CT number. The highest CT number (844.6 HU) was obtained at 15 mg/ml iodine with a tube current of 370 mA and an energy of 50 keV. The lowest CT number (65.4 HU) was obtained at 5 mg/ml iodine with a tube current of 200 mA and energy of 100keV.

The APE of the CT number of iodine from our in-house phantom and the standard is shown in Figure 5. Overall, the APE was <32% for all iodine concentrations. As the VMI energy increased, the APE became larger. The most accurate CT number measurement with the smallest APE (1.8%) was obtained with 15 mg/ml iodine at 50 keV.

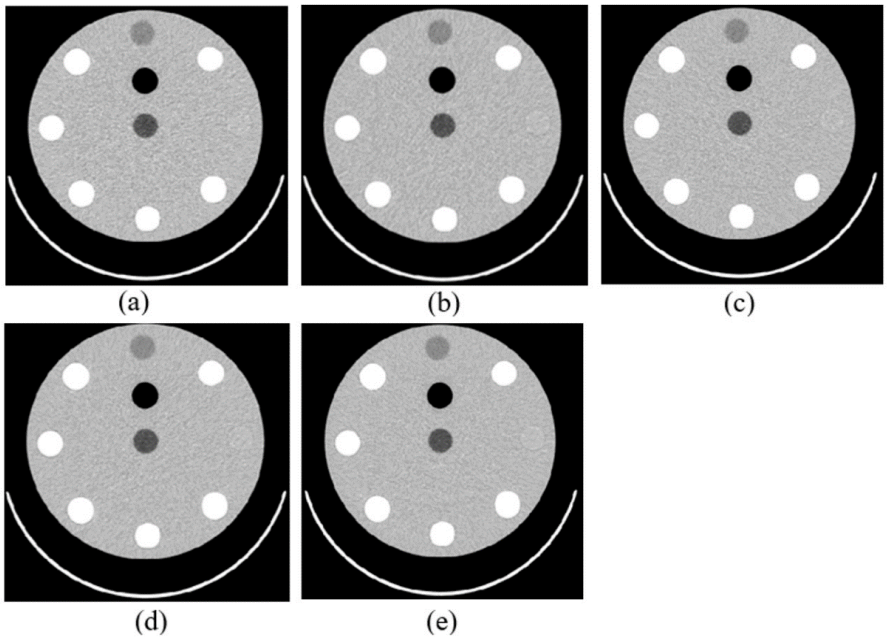


Figure 3. Virtual monochromatic images of the in-house phantom at energy level of 50 keV and tube voltage of 80/140 kV with various tube currents: (a) 200 mA, (b) 250 mA, (c) 300 mA, (d) 335 mA, and € 370 mA.

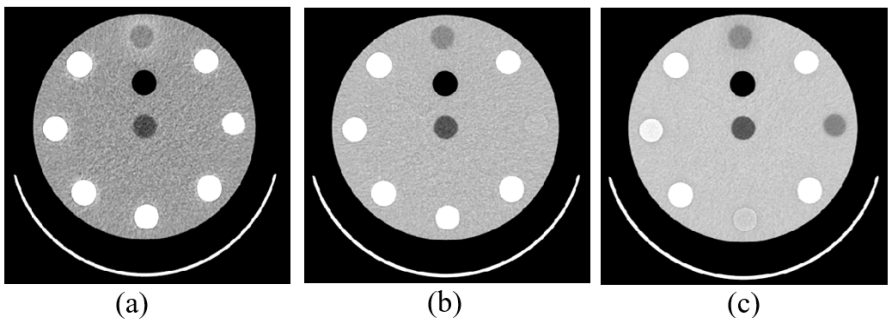


Figure 4. Virtual monochromatic images of the in-house at tube current 300 mA and tube voltage 80/140 kV with various energy levels: (a) 50 keV, (b) 70 keV, and (c) 100 keV.

DOI: https://doi.org/10.11113/jurnalteknologi.v89.25139

Table 3. CT number of iodine for various tube currents and VMI energy levels.

Iodine (mg/ml)	Energy (keV)	CT number (HU)					
		200 mA	250 mA	300 mA	335 mA	370 mA	Mean ± SD
5	50	306.4	306.8	307.6	308.3	309.2	307.7 ± 1.1
	70	146.5	149.7	149.9	150.6	152.2	149.8 ± 2.1
	100	65.4	66.3	67.4	68.2	68.5	67.2 ± 1.3
7.5	50	445.7	448.7	450.4	450.8	451.2	449.4 ± 2.2
	70	218.6	219.3	220.6	221.7	223.6	220.8 ± 1.9
	100	100.6	101.1	102.0	102.8	102.9	101.9 ± 1.0
10	50	565.7	572.8	576.4	577.1	585.8	575.6 ± 7.3
	70	280.2	280.6	281.3	281.8	282.0	281.2 ± 0.8
	100	128.4	128.8	129.1	130.0	132.7	129.8 ± 1.7
15	50	824.0	833.8	835.3	840.1	844.6	835.6 ± 7.7
	70	404.9	406.9	408.3	409.3	412.4	408.4 ± 2.8
	100	182.4	184.7	185.8	186.9	187.3	185.4 ± 1.9

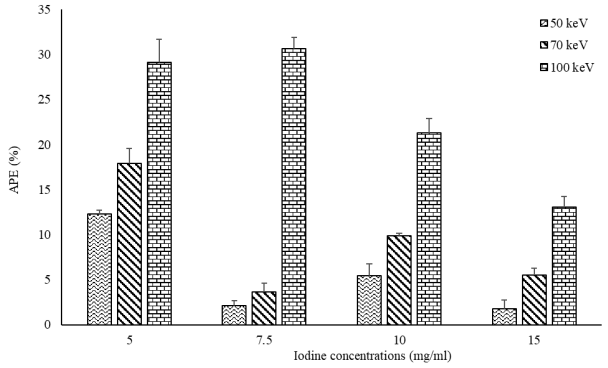


Figure 5. The graph of APE of CT number iodine for various iodine concentrations and VMI energy levels

3.3 CT number of calcium

The CT number of calcium for various tube currents and VMI energy levels are shown in Table 4. The change in the CT number of calcium shows the same trend as the CT number of iodine. The CT number of calcium increased as the tube current and concentration increased. The highest CT number (2090.7 HU) was obtained for 600 mg/ml calcium when the tube current was 370 mA and the energy was 50 keV. And the lowest CT number (511.6 HU) was obtained at 200 mg/ml calcium when the tube current was 200 mA and the energy was 100 keV.

The APE of the CT number of calcium from our in-house phantom and the standard is shown in Figure 6. The APE results are <25% for all calcium concentrations. The APE value at 200 mg/ml calcium showed the same trend as iodine, i.e., if the VMI energy increased, then the APE increased. However, with calcium concentrations of 300, 500, and 600 mg/ml, the increase in VMI energy caused a drastic decrease in APE. The most accurate CT number measurement with the smallest APE (2.1%) was obtained with 300 mg/ml calcium at 100 keV.

Table 4. CT number of calcium for various of tube currents and VMI energy levels.

Calcium (mg/ml)	Energy (keV)	CT number (HU)					
		200 mA	250 mA	300 mA	335 mA	370 mA	Mean ± SD
200	50	1321.1	1433.4	1448.2	1504.4	1531.1	1447.6 ± 81.2
	70	822.7	851.9	879.8	907.9	908.8	874.2 ± 37.1
	100	511.6	524.7	539.3	576.2	583.0	547.0 ± 31.4
300	50	1565.1	1570.3	1594.3	1639.4	1696.8	1613.2 ± 55.2
	70	909.7	913.0	934.3	950.9	954.0	932.4 ± 20.6
	100	630.4	631.8	633.2	646.6	646.8	637.8 ± 8.2
500	50	1845.7	1911.8	1914.7	1957.3	1977.3	1921.4 ± 50.6
	70	1119.3	1128.2	1142.5	1163.3	1164.2	1143.5 ± 20.2

DOI: https://doi.org/10.11113/jurnalteknologi.v89.25139

	100	725.2	726.0	730.8	738.5	739.7	732.0 ± 6.8
	50	2042.7	2075.3	2086.1	2089.3	2090.7	2076.8 ± 20.0
600	70	1219.8	1222.6	1228.7	1238.9	1240.8	1230.2 ± 9.4
	100	774.6	774.9	778.1	785.8	791.8	781.0 ± 7.5

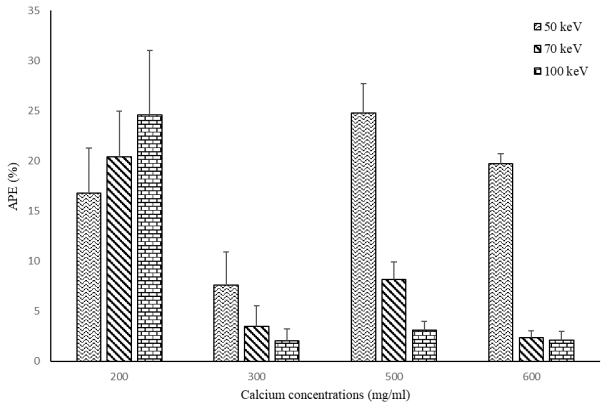


Figure 6. The graph of APE of CT number calcium for various calcium concentrations and VMI energy levels.

The availability of phantoms for DECT is essential for CT number accuracy testing. However, the standard phantoms are not yet available in some DECT centers in developing countries due to their high cost. The development of an alternative phantom using more economical materials could help hospitals monitor CT number accuracy on various materials.

In this study, an in-house phantom made of PESR and MEKP with iodine and calcium inserts of various concentrations, representing body tissues, was successfully developed. The PESR material was chosen because it has a density (ρ) of 1.21 g/cm^3 which is similar to acrylic so that it can be used as the main material for making phantoms. In addition, the PESR can withstand high temperature, has a relatively low price, and can be easily fabricated [18, 19]. Visually, the in-house phantom appeared homogeneous and had no air bubbles. Iopamidol ($C_{17}H_{22}I_3N_3O_8$) was used for iodine with various concentrations of 5, 7.5, 10, and 15 mg/ml representing intravenous contrast [14, 19]. It has high water solubility and low toxicity, so it is often used for CT examinations [20]. The calcium material was obtained from dilutions of calcium carbonate powder ($CaCO_3$). Calcium carbonate has a bone-like structure and properties. Calcium carbonate is the largest commercial source of calcium compounds [21]. Calcium concentrations of 200, 300, 500 and 600 mg/ml were used to represent bone mineral, CB-2 30%, CB-2 50% and cortical bone [14, 19].

Our in-house phantom was used to evaluate CT numbers of iodine and calcium at VMI energy levels of 50, 70, and 100 keV with tube current variation using DECT Ultrafast kV Switching. VMI in this energy range is often chosen as the standard image. VMIs at 50 keV can reduce beam hardening artifacts, which often occur in high-energy imaging. At 70 keV it is equivalent to the CT number in SECT of 120 kV. At 100 keV, there is no apparent enhancement of renal cysts [24]. The changes in CT numbers of calcium and iodine showed the same trend. As the tube current increased, the CT number also slightly increased (Tables 3 and 4). With increasing current, the penetration of X-rays into the tissue also increases, thus providing more information about the tissue composition and increasing the CT number. The attenuation coefficient is intrinsically dependent on the material and is independent of the number of photons passing through it. Therefore, although higher tube currents produce more photons and reduce noise, the CT number does not change drastically because the attenuation coefficient is the same [6, 25].

An evaluation of the CT number based on the energy level of VMI was conducted. CT number decreases by 1.5-3 times from an energy of 50 keV to 100 keV. In theory, at lower energies, the photoelectric effect is more dominant, especially for elements with higher atomic numbers such as iodine and calcium. This results in a higher CT number because the photoelectric effect contributes significantly to the attenuation. At high energies, Compton scattering dominates, making it less dependent on atomic number and resulting in a lower CT number [26]. Another reason is that when X-rays pass through tissue, the lower energy rays are absorbed more than the higher energy rays. This process is known as beam hardening, where the X-ray spectrum becomes harder (higher energy) as it passes through tissue. This can lead to a decrease in the CT number because the difference in attenuation between different tissues becomes less pronounced. DECT also enables better separation of different materials based on their attenuation properties at different energies. This enhanced differentiation can result in a lower average CT number when higher energy data is processed and combined with lower energy data. In summary, the decrease in CT number at higher energy levels in DECT is due to changes in the dominant attenuation mechanism, reduced beam hardening effect and more accurate material differentiation [26-28].

Based on the results of the current study, the APE in iodine is <32% (Figure 5) and in calcium it is <25% (Figure 6). The APE is more noticeable at low concentrations for both iodine and calcium, but there was a difference in APE dependence between

DOI: https://doi.org/10.11113/jurnalteknologi.v89.25139

iodine and calcium. At all iodine concentrations, the greater VMI energy,the greater the APE. With calcium concentrations of 300, 500, and 600 mg/ml, APE values decreased as VMI energy increased. At high energies, X-rays penetrate high-density materials such as calcium more easily. This reduces noise and artifacts so that CT number measurements are more consistent. Another reason is because at low energies, beam hardening can cause distortion to the CT number. At high energies, this effect is reduced and results in relatively accurate CT number measurements [29, 30].

Our in-house phantom serves as a practical alternative for hospitals lacking a standard QC phantom for DECT. Phantoms incorporating iodine and calcium allow for the testing of Hounsfield Unit (HU) consistency across different energies, which is crucial for assessing the accuracy of dual-energy detectors and algorithms. Furthermore, this phantom can help identify potential DECT-specific artifacts (like beam hardening in dense materials) under controlled conditions. Developing this in-house phantom is straightforward, requiring no specialized tools and using materials that are affordable and readily available. A 32 cm diameter version can also be developed to better simulate the size of a patient's body.

It is important to note that our in-house phantom significantly impacts training, routine QC, and patient safety in three key ways: training, routine QC, and patient safety. First, the phantom provides a readily available, controlled environment for hands-on training of technologists and physicists. Trainees can practice DECT acquisition protocols, learn to analyze dual-energy image datasets (e.g., virtual non-calcium images), and gain experience in identifying common DECT-specific artifacts (like beam hardening) before working with patients. Second, as an affordable alternative to commercial devices, the phantom enables hospitals to perform more frequent and accessible QC. By consistently checking HU consistency across energies using the iodine and calcium inserts, we ensure the accuracy of the dual-energy detectors and algorithms is maintained, which is vital for clinical results. Third, by guaranteeing the accuracy and stability of the DECT system through rigorous QC, the phantom minimizes the risk of diagnostic errors arising from equipment malfunction or drift. Furthermore, maintaining optimal system performance can potentially reduce the need for repeat scans, thereby limiting unnecessary radiation exposure to the patient.

Our study has limitations. We conducted the study using a single GE Revolution Ultrafast kV Switching DECT scanner limits the generalizability of the findings, as technical specifications vary across different vendors and models. Our primary goal, however, was to validate the phantom's efficacy as a site-specific, cost-effective QC alternative for hospitals utilizing similar single-source, fast kV-switching DECT technology. Regarding the material comparison, we recognize that the current in-house phantom only includes iodine and calcium inserts, which narrows the scope of validation. These materials were specifically chosen because they are the most critical components for testing the core dual-energy decomposition algorithms (e.g., bone/calcium removal and iodine quantification), which are central to DECT's clinical utility. While incorporating additional clinically relevant materials (e.g., adipose tissue or blood equivalents) would broaden the phantom's applicability, this initial design successfully validates its role in performing the fundamental QC checks necessary for maintaining accurate clinical performance on the target DECT system.

4.0 CONCLUSION

An in-house phantom with iodine and calcium inserts of various concentrations for QC of CT number of DECT has been successfully developed. Changes in CT number of iodine and calcium were not affected by tube current, but rather by the energy level of VMI. Overall, the APE of CT numbers of our phantom were <32% and <25% for iodine and calcium compared the to the standard at all concentrations. The APE value shows the compatibility between the DECT phantom and the standard phantom. Our in-house phantom can be used as an alternative phantom for QC of DECT if the standard phantom is not available.

Acknowledgement

This research was funded by the Riset Akselerasi Publikasi (RAP), Diponegoro University. Contract number: 222-236/UN7.D2/PP/IV/2025

Conflicts of Interest

The authors declare that there is no conflict of interest regarding the publication of this paper.

Data availability

The data supporting the findings of this study are available from the corresponding author upon reasonable request.

Ethics declaration

Formal ethical approval was not obtained for this study. However, the authors confirm that the research was conducted in accordance with established ethical principles and good research practices, with due consideration given to

DOI: https://doi.org/10.11113/jurnalteknologi.v89.25139

participant rights, informed consent, confidentiality, and responsible data handling.

References

[1] Schulz, R.A., Stein, J.A., Pelc, N.J. 2021. How CT Happened: The Early Development of Medical Computed Tomography. *Journal of Medical Imaging*. 8(5): 052110.

[2] McCollough, C.H. 2019. Computed Tomography Technology and Dose in the 21st Century. *Health Physics*. 116(2): 157-162.

[3] Kane, S.A., Gelman, B.A. 2020. *Introduction to Physics in Modern Medicine 3rd Edition*. Boca Raton: CRC Press.

[4] Agostini, A., Borgheresi, A., Mari, A., Floridi, C., Bruno, F. 2019. Dual-energy CT: Theoretical Principles and Clinical Applications. *Radiologica Medica*. 124: 1281-1295.

[5] Schmidt, B., and Flohr, T. 2020. Principles and Applications of Dual Source CT. *Physica Medica*. 79: 36-46.

[6] McCollough, C.H., Leng, S., Yu, L., Fletcher, J.G. 2015. Dual and Multi Energy CT: Principles, Technical Approaches and Clinical Applications. *Radiology*. 276(3): 637-653.

[7] Rajiah, P., Parakh, A., Kay, F., Baruah, D., Kambadakone, A.R., Leng, S. 2020. Update on Multienergy CT: Physics, Principles and Applications, *Radiographics*. 40(5): 1284-1308.

[8] Flohr, T.G., McCollough, C.H., Bruder, H., Petersilka, M. 2006. First performance evaluation of a dual-source CT (DSCT) System. *European Radiology*. 16: 256-268.

[9] Bogers, A.P., Antunes, C., Semedo, L.C. 2023. Pros and Cons of Dual Energy CT Systems: One does not fit all. *Tomography*. 9(1): 195-216.

[10] Tatsugami, T., Higaki, T., Nakamura, Y., Honda, Y., Awai, K. 2022. Dual Energy CT: Minimal essentials for radiologists. *Japanese Journal of Radiology*. 40(6): 547-559.

[11] Thieme, S.F., Graute, V., Nikolaou, K., Reiser, M.F., Hacker, M., Johnson, T.R.C. 2012. Dual Energy CT Lung Perfusion Imaging-Correlation with SPECT/CT. *European Journal of Radiology*. 81(2): 360-365.

[12] Hu, R., Besheli, L.D., Young, J., Wu, M., Pomerantz, S., Lev, M.H., Gupta, R., 2016. Dual-Energy Head CT Enables Acurate Distinction of Intraparenchymal Hemorrhage from Calcification in Emergency Department Patients. *Radiology*. 280(1): 177-83.

[13] Mar'ie, K., Lestariningsih, I., Nurley, Soejoko, D.S. 2019. Phantom Design for Analysis of CT Image Quality from Single Source and Dual Source CT Scan. *Journal of Physics: Conference Series*. 1568: 012019.

[14] Kojima, T., Shirasaka, T., Kondo, M., Kato, T., Nishie, A., Ishigami, K., Yabuuchi, H. 2021. A Novel Fast Kilovoltage Switching Dual Energy CT with Deep Learning: Accuracy of CT Number on Virtual Monochromatic Imaging and Iodine Quantification. *Physica Medica*. 81: 253-261.

[15] Fatichah, L., Anam, C., Sutanto, H., Naufal, A., Rukmana, D.A., Dougherty, G. 2023. Identification of the Computed Tomography Dose Index for Tube Voltage Variations in a Polyester Resin Phantom. *Applied Radiation and Isotopes*. 192: 110605.

[16] Shofiana, L.N., Anam, C., Sutanto, H., Asiah, R.H., Nihayati, R., Khaerul, A., Dogherty, G. 2021. Development of In-House Phantoms from Polyester Resin and Methyl Ethyl Ketone Peroxide Materials with Various Diameters: Investigation their CT numbers for Various Tube Voltage and Field of View, *Journal of Physics and Its Applications*. 4(1): 7-13.

[17] Camargo, G.E., Carneiro, G.N., Real, J.V., Doro, R.B., Malthez, A.I. 2023. Development of Phantom for Current Modulation Quality Assurance Test on Computed Tomography. *Radiation Protection Dosimetry*. 199(8): 1029-1033.

[18] Asiah, R.H., Sutanto, H., Anam, C., Arifin, Z., Bahrudin, Hilmawati, R. 2021. Development of In-House Head Computed Tomography Dose Index Phantoms Based on Polyester Resin Materials. *Iranian Journal of Medical Physics*. 18(4): 255-262.

[19] Yagi, M., Ueguchi, T., Koizumi, M., Ogata T., Yamada, S., Takahashi, Y., Sumida, I. 2013. Gemstone Spectral Imaging: Determination of CT to ED Conversion Curves for Radiotherapy Treatment Planning. *Journal of Applied Clinical Medical Physics*. 14(5): 173-186.

[20] Nusyirwan, Abral, H., Hakim, M., Vadia, R. 2019. The Potential of Rising Husk Fiber/Native Sago Starch Reinforced Biocomposite to Automotive Component, *IOP Conference Series: Materials Science and Engineering*. 602: 012085.

[21] Kartika, I.R., Kurniadewi, F., Nurjayadi, M., Rahmawati, Y. 2015. Pembuatan Case Gadget Chemistry Style. *Jurnal Sarwahita*. 12(2): 77-81.

[22] Rogers, D., Sheth, C., Eisenmenger, L., Mignogna, E. 2017. Iopamidol as an Oral Contrast Media for Computed Tomography: A Taste Comparison to Iohexol, Diatrioate sodium and Barium Sulfate. *Abdominal Radiology*. 42(1): 2822-2826.

[23] Riani. 2012. Evaluasi Radiografis Tinggi dan Densitas Tulang Alveolar pada Terapi Periodontitis dengan Allografi dibandingkan Xenograft. *Tesis*. Depok: Universitas Indonesia.

[24] Ohira, S., Karino, T., Nitta, Y., Hayashi, M. 2018. How Well Does Dual Energy CT with Fast Kilovoltage Switching Quantify CT Number and Iodine and Calcium Concentrations. *Academic Radiology*. 25(4): 519-528.

[25] Goo, H.W., and Goo, J.M. 2017. Dual-Energy CT: New Horizon in Medical Imaging. *Korean Journal of Radiology*. 18(4): 555-569.

[26] Coursey, C.A., Nelson, R.C., Boll, D.T., Paulson, E.K., Ho, L.M., Neville, A.M., Marin, D. 2010. Dual Energy Multidetector CT: How Does It Work, What Can It Tell Us, and When Can We Use It in Abdominopelvic Imaging?. *RadioGraphics*. 30(4): 1037-1052.

[27] Zhou, H., Zhang, L., Wang, Z., Gao, H. 2024. Fast KV-Switching and Dual-Layer Flat-Panel Detector Enabled Cone-Beam CT Joint Spectral Imaging. Physics in Medicine & Biology. 69: 115005.

[28] Topcuoglu, O and Sarikaya, B. 2019. Fast kilovoltage-switching dual energy CT offering lower x-ray dose than single energy CT for the chest: a quantitative and qualitative comparison study of the two methods of acquisition. *Diagn Interv Radiol*. 25(3): 204-209.

[29] Thomas, C., Schabel, C., Krauss, B., Weisel, K., Bongers, M., Claussen, C.D., Horger, M. 2015. Dual-Energy CT: Virtual Calcium Subtraction for Assessment of Bone Marrow Involvement of the Spine in Multiple Myeloma, *AJR Am J Roentgenol*. 204(3): W234-W331.

[30] Kumar, V., James, K., Xin H., Raman, S.V. 2017. Computation of Calcium Score with Dual Energy CT: A Phantom Study. *J Comput Assist Tomogr*. 41(1): 156–158.